LU TP 94-2

The Average Number of Sub-jets in a Hadron Collider Jet

Michael H. Seymour
Department of Theoretical Physics, University of Lund,
Sölvegatan 14A, S-22362 Lund, Sweden

Abstract

We calculate the average number of sub-jets in a jet, defined using a recently proposed jet clustering algorithm for hadron-hadron collisions. Our result is exact to leading order in α_s, and resums large leading and next-to-leading logarithms of the resolution variable, $y_{\rm cut}$, to all orders in α_s.

LU TP 94-2
February 1994

1 Introduction

In recent years, great progress has been made in QCD calculations of multi-parton processes, where resummation of large logarithmic terms must be performed to all orders, most notably in e^+e^- annihilation. This has the advantage of increasing the range of applicability of the predictions[1]. At the same time, it has been realised that not all quantities give perturbation series that can be resummed, and having a sequentially factorisable phase space has had to be added to the requirements of a 'good' observable. In particular, for jet rates and multiplicities to be resummed, distance measures of '$k_\perp$'-type must be introduced[2]. This has allowed resummed calculations of the jet multiplicity to be made[3].

Generalisations of the $k_\perp$ algorithm have also been proposed for deep inelastic scattering[4] and hadron-hadron collisions[5], and a resummed calculation has recently been completed for the former[6].

Studies of the hadron-hadron algorithm using a Monte Carlo event generator [5, 7] and next-to-leading order matrix elements[8] have shown a variety of advantages over more commonly used cone-type algorithms. It also has a two-scale form in which hard jets are defined at some large scale, and their internal structure resolved into sub-jets at some smaller scale. In this paper we calculate the multiplicity of such sub-jets. Our result is exact to leading order in α_s, and resums all leading and next-to-leading logarithms in the small resolution scale, $y_{\rm cut}$, even those suppressed by powers of the jet radius, R. We find that the multiplicity in a jet of a given flavour is largely independent of its production mechanism, and exhibits large differences between quark and gluon jets. It would therefore be a particular suitable variable with which to study such differences in a way that is under perturbative control.

In section 2 we define the particular variant of the $k_\perp$ jet clustering algorithm we shall be using, which defines jets inclusively, and then resolves their internal structure exclusively. In section 3 we calculate the multiplicity of sub-jets within a jet defined according to this algorithm, to leading order in α_s. Then, in section 4 we give results for the resummation of the large logarithmic terms associated with small $y_{\rm cut}$, and show how to match these with the leading-order calculation. In section 5 we present some numerical results for the sub-jet multiplicity. Of course our result is purely perturbative, and will suffer non-perturbative hadronisation effects. In section 6, we compare our result with the prediction of a Monte Carlo event generator that includes a model of hadronisation, to estimate the size of such effects. Finally in section 7 we make some concluding remarks.

2 The Jet Algorithm

The algorithm we use to define jets is the inclusive version of the $k_\perp$ algorithm for hadron-hadron collisions[5,8]. It proceeds according to the following steps,

1. For every pair of particles, define

$$d_{ij} = \min(p_{t,i}, p_{t,j})^2 \left\{(\eta_i - \eta_j)^2 + (\phi_i - \phi_j)^2\right\}, \tag{1}$$

where $p_{t,i}$, η_i and ϕ_i are the transverse momentum, pseudorapidity and azimuth of particle i. In addition, define for every particle

$$d_i = p_{t,i}^2 \, R^2, \tag{2}$$

where R is a parameter that plays the rôle of a jet radius in (η, ϕ) space, assumed to be of order 1.

2. Find the smallest member of $\{d_{ij}, d_i\}$, $d_{\min}$.

3. If $d_{\min} = d_{ij}$, merge particles i and j into a single pseudoparticle according to some recombination scheme, specified below. The algorithm continues from step 1, considering pseudoparticles on an equal footing with particles.

4. If $d_{\min} = d_i$, call pseudoparticle i a jet. Continue until there are no remaining pseudoparticles.

Note that in the soft and collinear limits d_{ij} reduces to the transverse momentum of the softer particle relative to the harder particle's direction, $k_\perp^2$.

It can be seen that a particle or pseudoparticle will be merged with its nearest neighbour if, and only if, their invariant opening angle is less than R. Thus the jets produced are phenomenologically rather similar to those defined by a cone-type algorithm. However, as a clustering algorithm of $k_\perp$-type, it has greatly improved theoretical properties.

As stressed in [8], this is a suitable way to define jets for a measurement of the inclusive jet cross-section, since the relevant large scale is measured from events. In contrast, the more exclusive methods discussed in [5] correspond to measuring event features at a chosen scale. Defining R to be exactly 1 is then particularly attractive, since the scale is then a global cut on the transverse momentum of emission, with initial-state and final-state radiation treated on an equal footing. This is also the value around which the scale-variation of the inclusive cross-section is smallest[8,9].

The idea of an inclusive jet definition is unappealing to proponents of QCD coherence, since jets can never be studied in isolation, but always as part of a coherent system. However, since this definition provides a strict cut on opening angles within the jet, it does allow such an isolation, at least to leading logarithmic accuracy. As we shall see, terms arise at next-to-leading logarithmic accuracy that violate this picture, although they disappear as the jet radius is made small. Nevertheless, they can be formulated in such a way as to be resummed.

Sub-jets are resolved within jet i by considering only those particles that ended up in it, and repeating steps 1 to 3, but stopping when all d_{jk} are above $d_{\text{cut}} \equiv y_{\text{cut}} p_{t,i}^2$. All remaining particles and pseudoparticles are called sub-jets.

We consider two recombination schemes. In the E-scheme the four-momenta of the particles are simply added,

$$p_{(ij)} = p_i + p_j. \tag{3}$$

Since the momenta become massive, the pseudorapidity in (1) must be replaced by the true rapidity, y, to preserve longitudinal boost invariance. The p_t-scheme is equivalent to what is often done in cone algorithms, and means that the jets remain massless, which is sometimes an advantage. The scalar transverse momentum is simply additive,

$$p_{t,(ij)} = p_{t,i} + p_{t,j}, \tag{4}$$

while the direction is given by the p_t-weighted sum,

$$\eta_{(ij)} = (p_{t,i}\eta_i + p_{t,j}\eta_j)/p_{t,(ij)}, \tag{5}$$

$$\phi_{(ij)} = (p_{t,i}\phi_i + p_{t,j}\phi_j)/p_{t,(ij)}. \tag{6}$$

Monte Carlo studies have not shown a strong preference for either scheme over the other[5, 7], so we consider both here.

3 Leading-order Calculation

The two-parton cross-section is given by

$$d\sigma_2 = \frac{(2\pi)^4}{(2(2\pi)^3)^2}\frac{1}{s\hat{s}} f_1(x_1)f_2(x_2)d\eta'\, p_t dp_t d\eta d\phi |\mathcal{M}_2|^2, \tag{7}$$

where $|\mathcal{M}_2|^2$ is assumed to contain the relevant sums and averages, and a sum over incoming partons is implicit. The lowest-order inclusive jet cross-section at a given phase-space point, (p_t, η, ϕ), is simply given by $d\sigma_2$ integrated over η', between the kinematic limits,

$$-\eta_{\max} < \eta' < \eta_{\max} \equiv \log(\sqrt{s}/p_t). \tag{8}$$

The three-parton cross-section is given by

$$d\sigma_3 = \frac{(2\pi)^4}{(2(2\pi)^3)^3}\frac{1}{s\hat{s}} f_1(x_1)f_2(x_2)d\eta'\, p_{t2}dp_{t2}d\eta_2 d\phi_2\, p_{t3}dp_{t3}d\eta_3 d\phi_3 |\mathcal{M}_3|^2, \tag{9}$$

where p_t ordering has been assumed, $p_{t3} < p_{t2} < p_{t1} \equiv |p_{t2} + p_{t3}|$.

We always use p_t for the scale in the structure functions and running coupling.

3.1 p_t-scheme

The final state we are interested in has two partons that are clustered together by the inclusive jet definition, giving a jet with given (p_t, η, ϕ). Thus they must be less than R apart in (η, ϕ) space. However, they are resolved by the sub-jet algorithm, with cutoff $d_{\rm cut} = y_{\rm cut} p_t^2$. Thus parton 3's $k_\perp$ relative to parton 2 must be greater than $\sqrt{y_{\rm cut}} p_t$. In the p_t-scheme the jet variables are given in terms of the sub-jet variables as

$$\begin{aligned} p_t &= p_{t2} + p_{t3}, && (10)\\ \phi &= \left(p_{t2}\phi_2 + p_{t3}\phi_3\right)/p_t, && (11)\\ \eta &= \left(p_{t2}\eta_2 + p_{t3}\eta_3\right)/p_t. && (12) \end{aligned}$$

We parameterise the two-body sub-space, $((p_{t2}, \eta_2, \phi_2), (p_{t3}, \eta_3, \phi_3))$ in terms of (p_t, η, ϕ) and the energy fraction $z = p_{t3}/(p_{t2} + p_{t3})$, the rescaled transverse momentum $y = k_\perp^2/p_t^2 = z^2\left((\phi_2 - \phi_3)^2 + (\eta_2 - \eta_3)^2\right)$, and an angle defined in (η, ϕ) space, φ. These give

$$\begin{aligned} p_{t2} &= (1-z)p_t, && (13)\\ \phi_2 &= \phi + \sqrt{y}\sin\varphi, && (14)\\ \eta_2 &= \eta + \sqrt{y}\cos\varphi, && (15)\\ p_{t3} &= z p_t, && (16)\\ \phi_3 &= \phi - \sqrt{y}\sin\varphi\frac{1-z}{z}, && (17)\\ \eta_3 &= \eta - \sqrt{y}\cos\varphi\frac{1-z}{z}. && (18) \end{aligned}$$

Note that in this form, it is clear that the rescaled transverse momentum, $\sqrt{y}$, is given by the opening angle between the jet axis and the axis of the harder sub-jet. It is possible that this is better determined experimentally than its usual definition, the product of the transverse momentum of the softer sub-jet and the opening angle between the two sub-jets.

The Jacobian transformation is

$$p_{t2}dp_{t2}d\eta_2 d\phi_2\; p_{t3}dp_{t3}d\eta_3 d\phi_3 = p_t dp_t d\eta d\phi\; d\varphi dy dz\; \frac{1-z}{2z}p_t^2. \qquad (19)$$

The kinematic limits are

$$\begin{aligned} 0 &< \varphi < 2\pi, && (20)\\ y_{\rm cut} &< y < R^2/4, && (21)\\ \sqrt{y}/R &< z < 1/2. && (22) \end{aligned}$$

Thus the two-sub-jet fraction is given by

$$R_2(y_{\rm cut};p_t,\eta,\phi) = \frac{\frac{(2\pi)^4}{(2(2\pi)^3)^3}p_t^3\int_{-\eta_{\rm max}}^{\eta_{\rm max}}d\eta'\int_0^{2\pi}d\varphi\int_{y_{\rm cut}}^{R^2/4}dy\int_{\sqrt{y}/R}^{1/2}dz\frac{1-z}{2z}\frac{1}{s\hat{s}}f_1(x_1)f_2(x_2)\,|\mathcal{M}_3|^2}{\frac{(2\pi)^4}{(2(2\pi)^3)^2}p_t\int_{-\eta_{\rm max}}^{\eta_{\rm max}}d\eta'\frac{1}{s\hat{s}}f_1(x_1)f_2(x_2)\,|\mathcal{M}_2|^2} \tag{23}$$

and the sub-jet multiplicity by

$$\mathcal{N}(y_{\rm cut};p_t,\eta,\phi) = 1 + R_2(y_{\rm cut};p_t,\eta,\phi). \tag{24}$$

3.2 *E*-scheme

We define z, y and φ in the same way, but use the E-scheme to recombine partons 2 and 3 into the jet. Thus we have

$$p_{t2} = (1-z)p_t\frac{1}{\sqrt{1-2z(1-z)(1-\cos(r\sin\varphi))}}, \tag{25}$$

$$\phi_2 = \phi + \tan^{-1}\left(\frac{z\sin(r\sin\varphi)}{z\cos(r\sin\varphi)+1-z}\right), \tag{26}$$

$$\eta_2 = \eta + \tanh^{-1}\left(\frac{z\sinh(r\cos\varphi)}{z\cosh(r\cos\varphi)+1-z}\right), \tag{27}$$

$$p_{t3} = zp_t\frac{1}{\sqrt{1-2z(1-z)(1-\cos(r\sin\varphi))}}, \tag{28}$$

$$\phi_3 = \phi_2 - r\sin\varphi, \tag{29}$$

$$\eta_3 = \eta_2 - r\cos\varphi, \tag{30}$$

where r is the solution of

$$y = \frac{p_{t3}^2r^2}{p_t^2} = \frac{z^2r^2}{1-2z(1-z)(1-\cos(r\sin\varphi))}. \tag{31}$$

The kinematic limits are given by

$$0 < \varphi < 2\pi, \tag{32}$$

$$y_{\rm cut} < y < y_{\rm max}, \tag{33}$$

$$z_{\rm min} < z < 1/2, \tag{34}$$

with

$$y_{\rm max} = \frac{R^2/4}{\frac{1}{2}(1+\cos(R\sin\varphi))}, \tag{35}$$

$$z_{\rm min} = \sqrt{y}/R\frac{\sqrt{1-y/R^2(1-\cos^2(R\sin\varphi))}-\sqrt{y}/R(1-\cos(R\sin\varphi))}{1-2y/R^2(1-\cos(R\sin\varphi))}. \tag{36}$$

Note that in the limits of small r and z that dominate the cross-section, the scheme is identical to the p_t-scheme, and that $y_{\max} > R^2/4$, $z_{\min} < \sqrt{y}/R$, so that the phase space is everywhere larger than in that scheme. The Jacobian transformation is also the same but with an extra factor of order 1,

$$p_{t2}dp_{t2}d\eta_2 d\phi_2\; p_{t3}dp_{t3}d\eta_3 d\phi_3 = p_t dp_t d\eta d\phi\; d\varphi dy dz\; \frac{1-z}{2z}p_t^2\; \times \\ \frac{1}{1-2z(1-z)(1-\cos(r\sin\varphi)) + rz(1-z)\sin(r\sin\varphi)\sin\varphi}. \tag{37}$$

Since these formulæ are so cumbersome, we only show the p_t-scheme when discussing analytical results, although we have made the analogous calculations in the E-scheme, and show numerical results in section 5.

3.3 Jet Flavours

The flavour of a jet is not well-defined beyond leading order calculations. Nevertheless, it will prove useful to be able to obtain sub-jet rates for individual jet flavours. We therefore proceed as follows.

In the two-parton matrix element the flavour of the detected jet is uniquely determined, and we can separate it into two pieces, $|\mathcal{M}_2^g|^2$ and $|\mathcal{M}_2^q|^2$ corresponding to gluons and quarks (meaning the sum of all quark and antiquark flavours). We define f_g and f_q to be their relative sizes, $f_g = |\mathcal{M}_2^g|^2/|\mathcal{M}_2|^2$, $f_q = |\mathcal{M}_2^q|^2/|\mathcal{M}_2|^2$, such that $f_g + f_q = 1$. We also define the integrated fractions

$$F_g = \frac{\int_{-\eta_{\max}}^{\eta_{\max}} d\eta' \frac{1}{s\hat{s}} f_1(x_1) f_2(x_2)\; |\mathcal{M}_2^g|^2}{\int_{-\eta_{\max}}^{\eta_{\max}} d\eta' \frac{1}{s\hat{s}} f_1(x_1) f_2(x_2)\; |\mathcal{M}_2|^2}, \tag{38}$$

and likewise for F_q, so that $F_g + F_q = 1$.

In the three-parton case, the two partons that are clustered to make the jet can be in any of three flavour states: 'gluon', i.e. gluon+gluon or quark+antiquark; 'quark', i.e. quark+gluon; or 'other', i.e. quark+quark or quark+antiquark'. Note that 'other' does not give rise to any large logarithms, and the cross-section is dominated by 'quark' and 'gluon' jets.

It is important to stress that the main results we show do not rely on this unphysical separation, but are simply the full three-body cross-section divided by the full two-body cross-section.

3.4 Large Logarithmic Terms

In the limit of small y_{cut}, R_2 will be given by the leading and next-to-leading logarithmic terms. In order to be able to match to the resummed calculation, we

would like to extract these terms, and treat them analytically. Doing so will also improve the convergence of the integral, which we perform numerically.

To next-to-leading logarithmic accuracy, the integrand of the numerator of (23) can be approximated by

$$\frac{dy}{y} dz \left(\frac{u}{z} - \frac{v}{2} \right), \tag{39}$$

where u and v are constants to be defined shortly. This can be integrated to give

$$\begin{aligned} &\int_{y_{\rm cut}}^{R^2/4} \frac{dy}{y} \int_{\sqrt{y}/R}^{1/2} dz \left(\frac{u}{z} - \frac{v}{2} \right) \\ &= \frac{1}{4} \left(u \log^2 Y + (v + 2u \log 4) \log Y + u \log^2 4 + v(2 - 4\sqrt{Y} + \log 4) \right), \end{aligned} \tag{40}$$

where $Y = y_{\rm cut}/R^2$.

We can use this to improve the convergence of the integral, by subtracting the approximated integrand from $|\mathcal{M}_3|^2$, and adding the right-hand-side of (40) after integration to give back the full integral. We define

$$|\mathcal{M}_3'|^2 = |\mathcal{M}_3|^2 - \frac{16\pi\alpha_{\rm S}}{p_t^2} \frac{u - vz/2}{1 - z} \frac{1}{y} |\mathcal{M}_2|^2, \tag{41}$$

where u and v are chosen to match the leading and next-to-leading logarithmic behaviour of $|\mathcal{M}_3|^2$. In order to account for the mixture of jets at each phase-space point, the coefficients for quark jets, U_q, V_q, and gluon jets, U_g, V_g, should be weighted by the flavour fractions f_q and f_g defined earlier. So we set

$$u = f_q U_q + f_g U_g, \tag{42}$$

$$v = f_q V_q + f_g V_g. \tag{43}$$

We define a corresponding R_2' by replacing $|\mathcal{M}_3|^2$ by $|\mathcal{M}_3'|^2$ in (23). After using (40) to integrate over z, y and the trivial φ, the only non-constants multiplying $|\mathcal{M}_2|^2$ are f_q and f_g, so they give the integrated flavour fractions F_q and F_g. R_2 is therefore given by

$$\begin{aligned} &R_2(y_{\rm cut}; p_t, \eta, \phi) = R_2'(y_{\rm cut}; p_t, \eta, \phi) + \\ &\quad \frac{\alpha_{\rm S}}{4\pi} \left(U \log^2 Y + (V + 2U \log 4) \log Y + U \log^2 4 + V(2 - 4\sqrt{Y} + \log 4) \right), \end{aligned} \tag{44}$$

where

$$U = F_q U_q + F_g U_g, \tag{45}$$

$$V = F_q V_q + F_g V_g. \tag{46}$$

4 Resummation of Large Logarithmic Terms

4.1 Final-state Emission

Large logarithmic terms of leading and next-to-leading type arise at all orders in the cross-section due to final-state emission. By explicitly setting up the evolution equations, one easily finds that they are identical to the final state of e^+e^- annihilation at scale $p_t R$ with cutoff $p_t\sqrt{y_{\rm cut}}$. However, at next-to-leading logarithmic accuracy, the overall energy scale is not fixed, only the ratio of the upper and lower scales, so we use this freedom to define the scale as $Q = p_t$ and cutoff as $Q_0 = p_t\sqrt{y_{\rm cut}}/R$. This makes the matching with the leading-order result more natural, since that uses p_t for the scale in α_s. The multiplicity of sub-jets in a gluon and quark jet respectively is then given by[3]

$$\mathcal{N}_g(Q_0,Q) = \mathcal{N}^+(z_0,z_1) + 2\frac{a-b}{b}\tilde{\mathcal{N}}(z_0,z_1), \tag{47}$$

$$\begin{aligned}\mathcal{N}_q(Q_0,Q) &= \left(1-\frac{C_F}{C_A}\right)\mathcal{N}^-(z_0,z_1) + \frac{C_F}{C_A}\Big[\mathcal{N}^+(z_0,z_1) \\ &\quad +2\frac{2a-b-3C_A}{b}\tilde{\mathcal{N}}(z_0,z_1)\Big],\end{aligned} \tag{48}$$

where

$$\mathcal{N}^+(z_0,z_1) = z_1\left(\frac{z_0}{z_1}\right)^B \left[I_{B+1}(z_1)K_B(z_0) + K_{B+1}(z_1)I_B(z_0)\right], \tag{49}$$

$$\mathcal{N}^-(z_0,z_1) = \left(\frac{z_0}{z_1}\right)^{\frac{8}{3}\frac{C_F}{C_A}\frac{N_f}{b}}, \tag{50}$$

$$\tilde{\mathcal{N}}(z_0,z_1) = \left(\frac{z_0}{z_1}\right)^B \left[I_B(z_1)K_B(z_0) - K_B(z_1)I_B(z_0)\right], \tag{51}$$

with

$$z_0 = \sqrt{\frac{32\pi C_A}{b^2\alpha_s(Q_0)}}, \tag{52}$$

$$z_1 = \sqrt{\frac{32\pi C_A}{b^2\alpha_s(Q)}}, \tag{53}$$

and

$$B = a/b, \tag{54}$$

$$a = \frac{11}{3}C_A + \frac{2N_f}{3} - \frac{4C_F N_f}{3C_A}, \tag{55}$$

$$b = \frac{11}{3}C_A - \frac{2N_f}{3}. \tag{56}$$

Note that in the threshold region (the region where $\alpha_s \log^2 y_{cut}$ is small but $\log y_{cut}$ is still large), these have expansions

$$\mathcal{N}_g = 1 + \frac{\alpha_s}{4\pi}\left[C_A \log^2 Y + b \log Y\right] + \mathcal{O}(\alpha_s^2), \quad (57)$$

$$\mathcal{N}_q = 1 + \frac{\alpha_s}{4\pi}\left[C_F \log^2 Y + 3C_F \log Y\right] + \mathcal{O}(\alpha_s^2), \quad (58)$$

where $Y = y_{cut}/R^2$.

4.2 Soft Emission

In addition to soft and collinear emission within the jet, the multiplicity is increased by soft emission from elsewhere in the event that happens to lie close enough to the jet to be combined with it. Although this is suppressed by the area of the jet, R^2, it gives rise to a logarithm of y_{cut} at leading order, and thus must be included in our resummation. However, it is clear that the probability for such emission does not factorise into the jet evolution, but depends on the flavours and kinematics of the entire event. It is therefore a surprise that such terms can be systematically resummed to all orders, as we shall see.

First we consider a simple analogy with a two-jet event in e^+e^- annihilation, where there is a single well-defined colour current. We use our jet algorithm at a large angle to the event axis and calculate the leading term of the number of gluons reconstructed, ($r^2 \equiv y^2 + \phi^2$),

$$\mathcal{N} = \frac{C_F}{\pi^2}\int \frac{dq_t}{q_t}\alpha_s(q_t)\int dy \int d\phi\ \Theta(R-r)\ \Theta(q_t r - p_t)\ \Theta(p_t - q_t) \quad (59)$$

$$= \frac{C_F}{\pi} R^2 \int_{Q_0}^{p_t} \frac{dq_t}{q_t}\alpha_s(q_t) \quad (60)$$

$$\approx -\frac{C_F \alpha_s(p_t)}{2\pi} R^2 \log Y. \quad (61)$$

Note that this depends only on the colour factor, C_F, and on parameters of the jet, p_t, R and Y, but not of the whole event.

Now consider calculating the same quantity to second order in α_s, and next-to-leading logarithmic accuracy. Two contributions arise: the emission of a second soft gluon into the jet, and the splitting of the leading order gluon. The former is $\sim R^4\alpha_s^2 \log^2$, and is therefore next-to-next-to-leading, and thus negligible. However, if the splitting is both soft and collinear it contributes two logarithms to give $\sim R^2\alpha_s^2 \log^3$. It can be seen that this structure will continue to all orders and, to next-to-leading logarithmic accuracy, the additional multiplicity is given by the convolution of the first-order probability with the resummed multiplicity of a gluon jet,

$$\mathcal{N} = C_F R^2 \int_{Q_0}^{p_t} \frac{dq_t}{q_t}\frac{\alpha_s(q_t)}{\pi}\mathcal{N}_g(Q_0, q_t). \quad (62)$$

This integral can be rewritten using the leading logarithmic evolution equation, to give

$$\mathcal{N} = C_{\rm F} R^2 \frac{\mathcal{N}'_g(Q_0, Q)}{2C_{\rm A}}, \tag{63}$$

where $\mathcal{N}'_g(Q_0, Q) \equiv Q\frac{d}{dQ}\mathcal{N}_g(Q_0, Q)$. We use the double-logarithmic approximation for $\mathcal{N}'_g$, since this is sufficient to retain next-to-leading logarithmic accuracy overall, while avoiding the practical problems that would be caused by the next-to-leading result (47) being non-monotonic for $Q \sim Q_0$. It also avoids subtleties related to the flavour-dependence that would arise in (62) if the next-to-leading kernel were used. Thus, in terms of the parameters defined earlier, we have

$$\mathcal{N}'_g(Q_0, Q) = \frac{8C_{\rm A}}{bz_1}\sinh(z_1 - z_0). \tag{64}$$

Returning now to hadron-hadron collisions, we see that the 'colour factor' appearing in (63) is not well defined—it is a function of both the flavours and dynamics of the hard scattering. A rough guide to its size can be found by considering the small $\hat{t}$ and $\hat{u}$ limits of each colour amplitude, the most important of which give $\sim C_{\rm F}$ for quark jets and $\sim \frac{1}{2}C_{\rm A}$ for gluon jets. Numerically we find that these are about right. However, we only use these approximate values to improve the convergence of the integral, and it is the exact result of this integral that is used in the final answer. This then effectively gives us the single logarithmic term equivalent to (61). We can then resum the associated next-to-leading logarithmic terms to all orders, simply by multiplying this integral by the factor

$$\frac{\mathcal{N}'_g(p_t\sqrt{Y}, p_t)}{-C_{\rm A}\alpha_{\rm S}(p_t)/\pi \log Y}, \tag{65}$$

to give the equivalent of (63). This factor rises slowly from unity as Y becomes much smaller than one.

4.3 Matching with the Leading-order Calculation

By comparing (44) with (57,58), it is clear that the resummed final-state logarithms can be combined analytically with the leading-order result, simply by setting

$$U_g = C_{\rm A}, \tag{66}$$
$$V_g = b - 2U_g \log 4, \tag{67}$$
$$U_q = C_{\rm F}, \tag{68}$$
$$V_q = 3C_{\rm F} - 2U_q \log 4, \tag{69}$$

and adding the entire resummed result instead of the leading part. The soft next-to-leading logarithms can be resummed simply by multiplying what remains of the

leading-order cross-section after the final-state logarithms have been subtracted, by the factor given in (65). That is, we write

$$\mathcal{N}(y_{\rm cut};p_t,\eta,\phi) \;=\; F_g\mathcal{N}_g(p_t\sqrt{Y},p_t) \;+\; F_q\mathcal{N}_q(p_t\sqrt{Y},p_t) \;+ \\ \left[R_2'(y_{\rm cut};p_t,\eta,\phi)+\frac{\alpha_{\rm S}}{4\pi}\left(U\log^2 4+V\left(2-4\sqrt{Y}+\log 4\right)\right)\right]\frac{\mathcal{N}_g'(p_t\sqrt{Y},p_t)}{-C_{\rm A}\alpha_{\rm S}/\pi\log Y}. \quad (70)$$

This result is exact to leading order in $\alpha_{\rm S}$, and next-to-leading order in logarithms of $Y = y_{\rm cut}/R^2$.

We finally note that in our approach, Y is assumed to be the only small parameter. Additional large logarithmic terms will arise for small R, as well as for the extreme kinematic regimes of large rapidity or small p_t, so our result should only be used well away from those extremes.

5 Numerical Results

We have adapted a version of the NJETS matrix-element Monte Carlo package[10] to calculate the sub-jet multiplicity for any desired configuration.

There is no appreciable dependence of the sub-jet multiplicity of a given jet flavour on the parton distribution set used. There is a weak dependence of the total sub-jet multiplicity due to small differences in the predicted ratios of gluon to quark jets in the inclusive jet sample, but we have found this to be small over most of phase-space, so we do not show individual graphs for each set. Instead we choose Duke and Owens set 1[11]. This uses a Λ value of 200 MeV, which we also use for the running coupling.

The results are shown in fig. 1, for a central 100 GeV jet in a $\rm p\bar{p}$ collision at $\sqrt{s} = 1.8$ TeV, with $R = 1$ in the p_t-scheme (these are the parameters we use for all graphs, except where stated otherwise). We see that resumming the leading and next-to-leading logarithms is essential for small $y_{\rm cut}$ values, and even for intermediate values around 0.01 makes a significant difference. The soft next-to-leading logarithms are just as important as the final-state leading logarithms in the intermediate $y_{\rm cut}$ range although they become relatively less important at small $y_{\rm cut}$. In the intermediate region, we would expect that most of the correction given by our resummation would actually be reproduced by a next-to-leading fixed-order calculation, since $\alpha_{\rm S}\log^2 y_{\rm cut}$ is not too large there.

In fig. 2 we show the value of the integral performed by the Monte Carlo program. The Monte Carlo errors are strongly correlated between the different curves and $y_{\rm cut}$ values, so only one is shown to set the overall scale. The integral is rather flat in $y_{\rm cut}$, showing that our guess of the size of the soft logarithm is quite accurate. Comparing this graph with fig. 1, we see that only a tiny fraction of the final answer comes from this integral, and the majority comes from the analytically treated logarithms and finite terms.

In fig. 3 we show the sub-jet multiplicity in quark and gluon jets separately, which is much as one would expect. Although the leading logarithms give a ratio of $C_A/C_F = 9/4$ for the multiplicities, this is reduced by the next-to-leading logarithmic terms, particularly the soft logarithm, which is almost identical for quark and gluon jets. The 'other' jet contribution is not visible in fig. 3 because it is so small. It has no logarithmic part, so is entirely given by the dotted line in fig. 2, which is clearly completely insignificant.

Fig. 4 shows the difference between the two recombination schemes, which is small. It might appear from the definitions of section 3.2 that the multiplicity should be larger in the E-scheme than the p_t-scheme. However, the E-scheme requires the vector sum of the sub-jet momenta to be equal to the jet momentum, while the p_t-scheme requires their scalar sum to be equal to it. Thus any given point in the sub-jet phase space corresponds to a larger sub-process energy in the E-scheme, and so a smaller cross-section. Since the schemes become identical in the dominant regions of phase space, this difference is small.

In fig. 5 we show the p_t dependence of the sub-jet multiplicity for two representative $y_{\rm cut}$ values. For quark and gluon jets, this is almost entirely due to the running coupling. The average sub-jet multiplicity interpolates between them as the relative rate of quark and gluon jets changes with p_t. Note that the inclusive jet rate falls by about ten orders of magnitude over this p_t range.

In any inclusive jet algorithm, one would hope that the properties of the detected jet are as independent of the production mechanism as possible. As we see in figs. 6 and 7 this is indeed the case for our algorithm. Note that the kinematic limit for a 100 GeV jet in a 1.8 TeV collision is about $|\eta| = 2.9$, so it is not too surprising that the jet gets squeezed near to that rapidity.

6 Hadronisation

We have used the HERWIG Monte Carlo event generator[12], version 5.7, to simulate the non-perturbative contributions to the sub-jet multiplicity. The parameters of the hadronisation model give a good overall fit to data from e^+e^- annihilation at the Z peak. The simple underlying event model, based on a parameterisation of minimum bias events, gives at least qualitative agreement with hadron collider jets. We leave all parameters at their default values.

The result is shown in fig. 8, and is very similar to that shown in [3] for e^+e^- annihilation. The parton-level output from HERWIG is in reasonable agreement with the analytical result down to $y_{\rm cut} \sim 10^{-4}$. This corresponds to a momentum scale of 1 GeV, which is about the infrared cutoff value used in HERWIG. The effect of this cutoff can be clearly seen. However, the result using the hadrons that come from the hard interaction rises above the perturbative prediction at a $y_{\rm cut}$ value corresponding to a few GeV. This seems to be a universal prediction of the cluster hadronisation model. It would certainly be interesting to measure sub-jets

in this region, with the hope of learning more about the onset of hadronisation. The additional hadrons coming from the model of the underlying event do not have as large an effect, but do increase the sub-jet multiplicity a little.

In addition to affecting the average sub-jet multiplicity, hadronisation effects will cause event-to-event fluctuations in the scales at which sub-jets are resolved. As shown in [5], these fluctuations are somewhat larger than those found in e^+e^- annihilation, and it seems that comparisons with perturbative calculations will become difficult for sub-jet scales below about 10 GeV. Although the jet and sub-jet definitions used there are slightly different to this one, we would not expect the conclusion to be significantly different with this algorithm. Nevertheless, as just mentioned, there is much to be learned from this region, for example in comparing sub-jet distributions at very small scales with the equivalent hadron distributions.

7 Conclusion

The introduction of $k_\perp$-type algorithms for hadron-hadron collisions makes possible many theoretical improvements in the QCD predictions for jet rates and properties.

In this paper we have concentrated on one particular property of jets that are inclusively defined in this algorithm, the multiplicity of sub-jets within them. At large $y_{\rm cut}$, this would provide a new way to measure α_s in hadron-hadron collisions. However, for this to be theoretically attractive, next-to-leading order predictions would be needed, both because the renormalisation scheme/scale is not well defined in leading order calculations, and because we expect the corrections to be numerically important.

At small $y_{\rm cut}$, the $k_\perp$ algorithm has the great advantage that leading and next-to-leading logarithms of $y_{\rm cut}$ can be systematically resummed to all orders. This is even true of the next-to-leading logarithms that are suppressed by powers of the jet radius, which arise due to soft emission from elsewhere in the event.

In both the small and large $y_{\rm cut}$ regions, large differences between quark and gluon jets are predicted. In addition, the sub-jet multiplicity in a jet of a given flavour and given transverse momentum is predicted to be almost independent of the jet's production mechanism, i.e. its rapidity, the energy of the collision, the colliding beam types, parton distributions, etc. Thus it seems that this sub-jet multiplicity would be an ideal area in which to look for quark/gluon jet differences that are under perturbative control.

Acknowledgments

It is a pleasure to acknowledge numerous discussions with Stefano Catani, Yuri Dokshitzer and Bryan Webber on these and related subjects. I am also grateful to the organisers of the Cambridge meeting of the European Collider Physics Network where this work was begun.

References

1. See for example:
   S. Catani, L. Trentadue, G. Turnock, B.R. Webber, Nucl.Phys.B407(1993)3;
   ALEPH Collaboration, D. Decamp et. al., Phys. Lett. B284 (1992) 163;
   OPAL Collaboration, P.D. Akrawy et. al., Z. Phys. C. 59 (1993) 1;
   DELPHI Collaboration, P. Abreu et. al., Z. Phys. C. 59 (1993) 21;
   and references therein.

2. S. Catani, Yu.L. Dokshitzer, M. Olsson, G. Turnock and B.R. Webber, Phys. Lett. B269 (1991) 432

3. S. Catani, Yu.L. Dokshitzer, F. Fiorani and B.R. Webber, Nucl. Phys. B377 (1992) 445

4. S. Catani, Yu.L. Dokshitzer and B.R. Webber, Phys. Lett. 285B (1992) 291

5. S. Catani, Yu.L. Dokshitzer, M.H. Seymour and B.R. Webber, Nucl. Phys. B406 (1993) 187

6. S. Catani, Yu.L. Dokshitzer and B.R. Webber, CERN preprint CERN-TH.7099/93

7. M.H. Seymour, Lund preprint LU TP 93/8, to appear in Z. Phys. C.

8. S.D. Ellis and D.E. Soper, Phys. Rev. D48 (1993) 3160

9. S.D. Ellis, Z. Kunszt and D.E. Soper, Phys. Rev. Lett. 69 (1992) 3615

10. F.A. Berends, W.T. Giele, H. Kuijf, Nucl. Phys. B333 (1990) 120;
    F.A. Berends and H. Kuijf, Nucl. Phys. B353 (1991) 59

11. D.W. Duke and J.F. Owens, Phys. Rev. D30 (1984) 49

12. G. Marchesini, B.R. Webber, G. Abbiendi, I.G. Knowles, M.H. Seymour and L. Stanco, Comp. Phys. Commun. 67 (1992) 465

Figure Captions

Figure 1: The multiplicity of sub-jets in a 100 GeV jet according to the leading-order matrix element (dashed), resummed final-state logs (dotted), matched leading-order and final-state logs (dot-dashed) and the full result with matched leading-order and leading and next-to-leading logs (solid). (a) and (b) are identical, but on different axes.

Figure 2: The result of the integration that is used to obtain the multiplicity of sub-jets in a 100 GeV jet (solid), which is also broken down by flavour into gluon (dashed), quark (dot-dashed), and 'other' (dotted) jets. The single Monte Carlo error bar shown is indicative of those on each point of each curve, which are all strongly correlated.

Figure 3: The multiplicity of sub-jets in a 100 GeV jet (solid), which is also broken down by flavour into gluon (dashed) and quark (dot-dashed) jets.

Figure 4: The multiplicity of sub-jets in a 100 GeV jet in the p_t-scheme (solid) and E-scheme (dashed).

Figure 5: The multiplicity of sub-jets in a jet as a function of its transverse momentum, broken down by flavour. Curves are as in fig. 3.

Figure 6: The multiplicity of sub-jets in a 100 GeV jet as a function of its rapidity, broken down by flavour. Curves are as in fig. 3.

Figure 7: The multiplicity of sub-jets in a 100 GeV jet as a function of the centre-of-mass collision energy, broken down by flavour. Curves are as in fig. 3. The barely discernible pairs of curves are for pp and $\mathrm{p\bar{p}}$ collisions.

Figure 8: The multiplicity of sub-jets in a 100 GeV jet according to the analytical result (solid), and HERWIG at parton level (dashed), using only hadrons from the hard interaction (dotted) and using all hadrons (dot-dashed),

Figure 1a

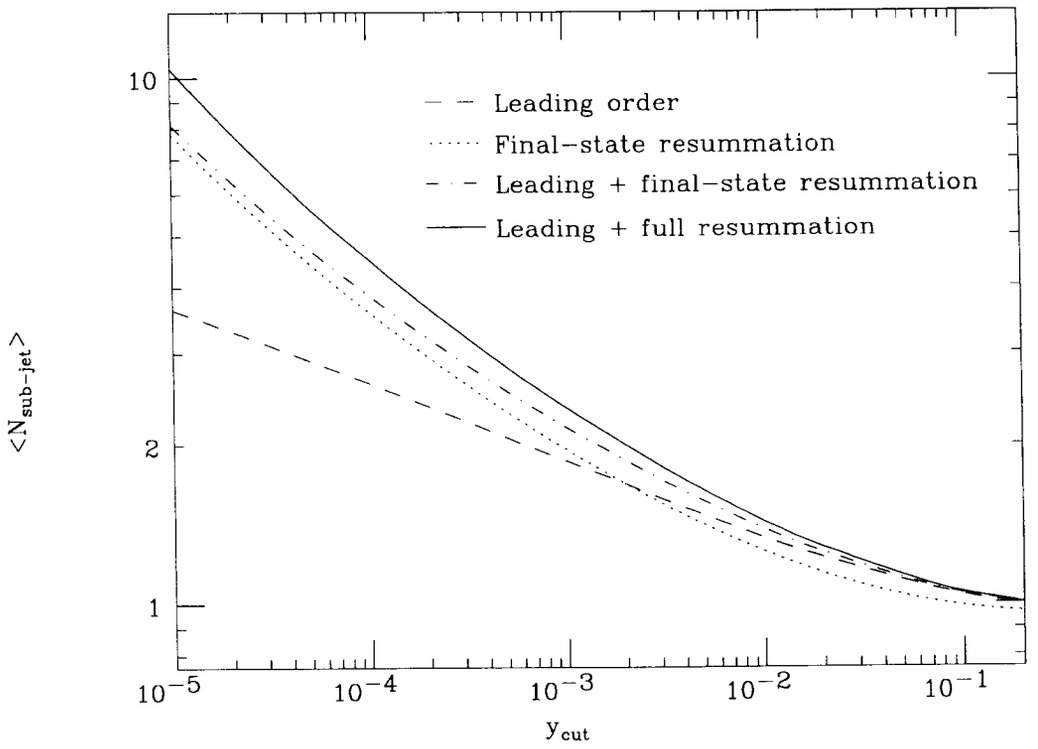

Figure 1b

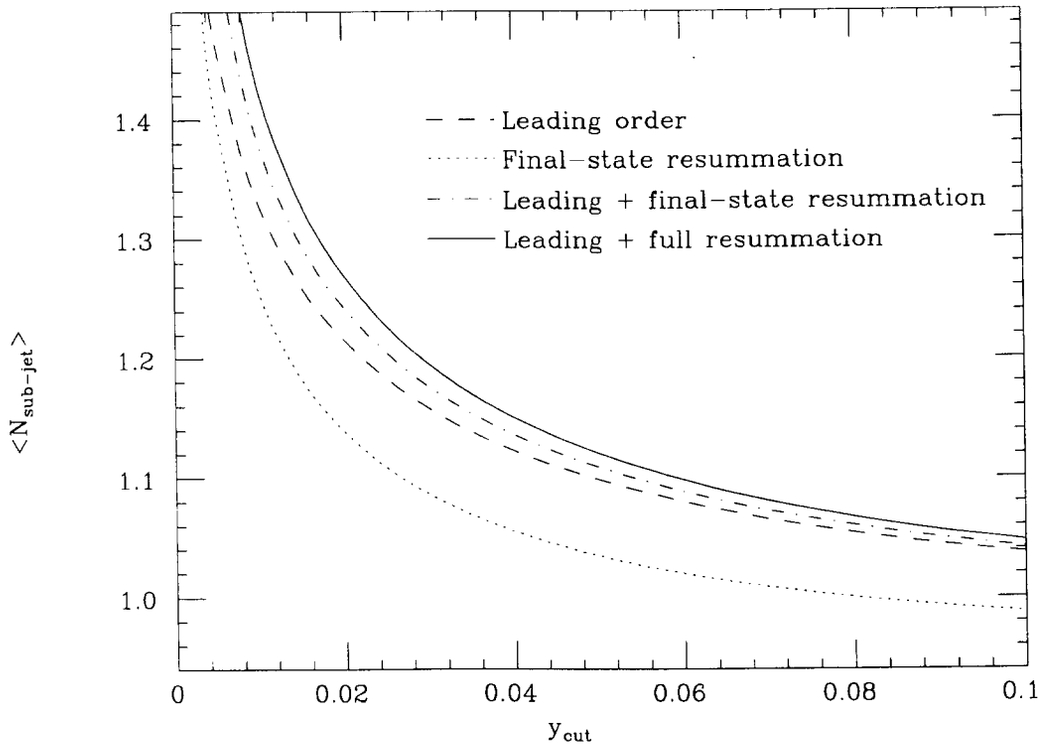

Figure 2

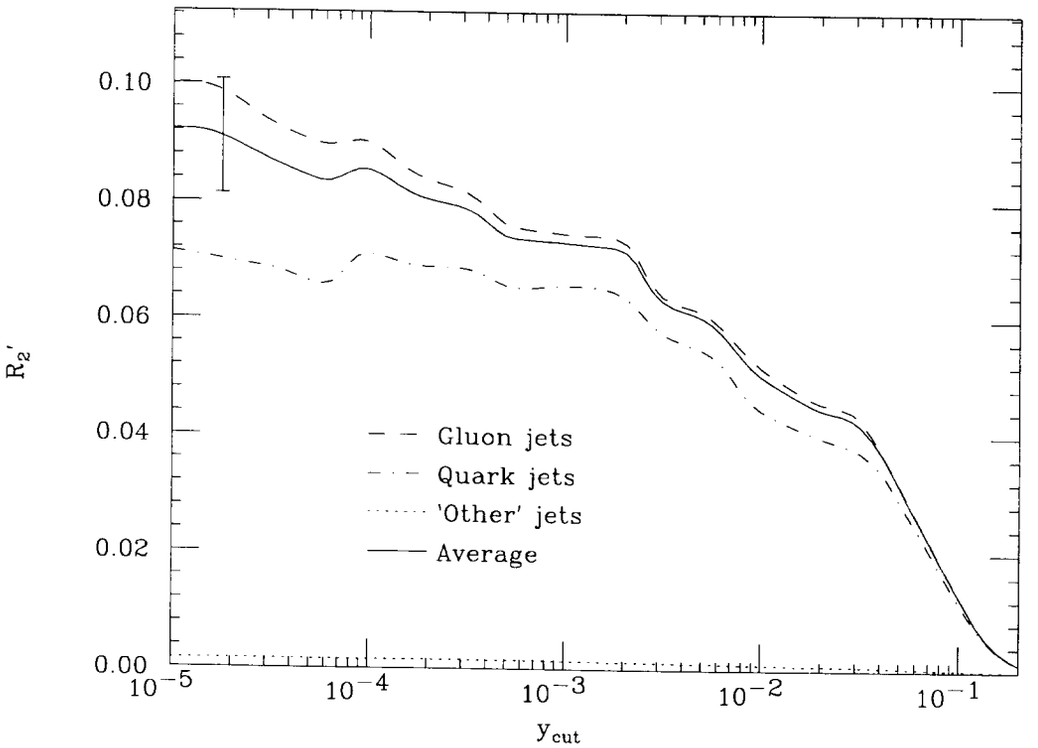
0.10
0.08
0.06
0.04
0.02
0.00
R_2'
10^{-5}
10^{-4}
10^{-3}
10^{-2}
10^{-1}
y_{cut}
Gluon jets
Quark jets
'Other' jets
Average

Figure 3a

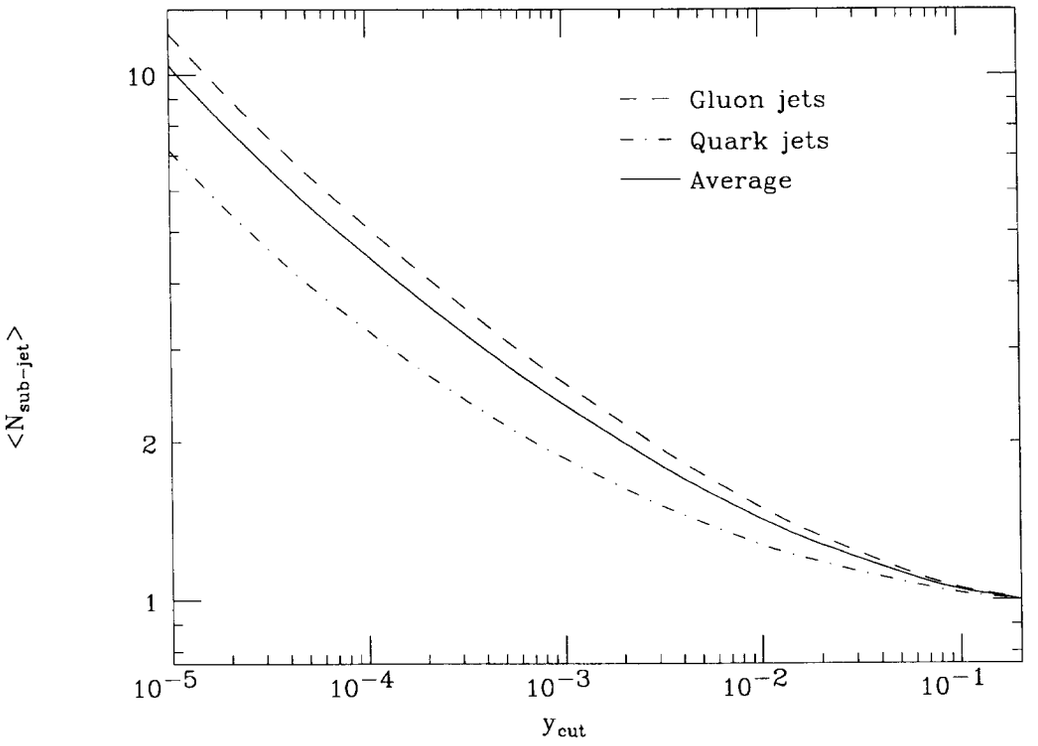

Figure 3b

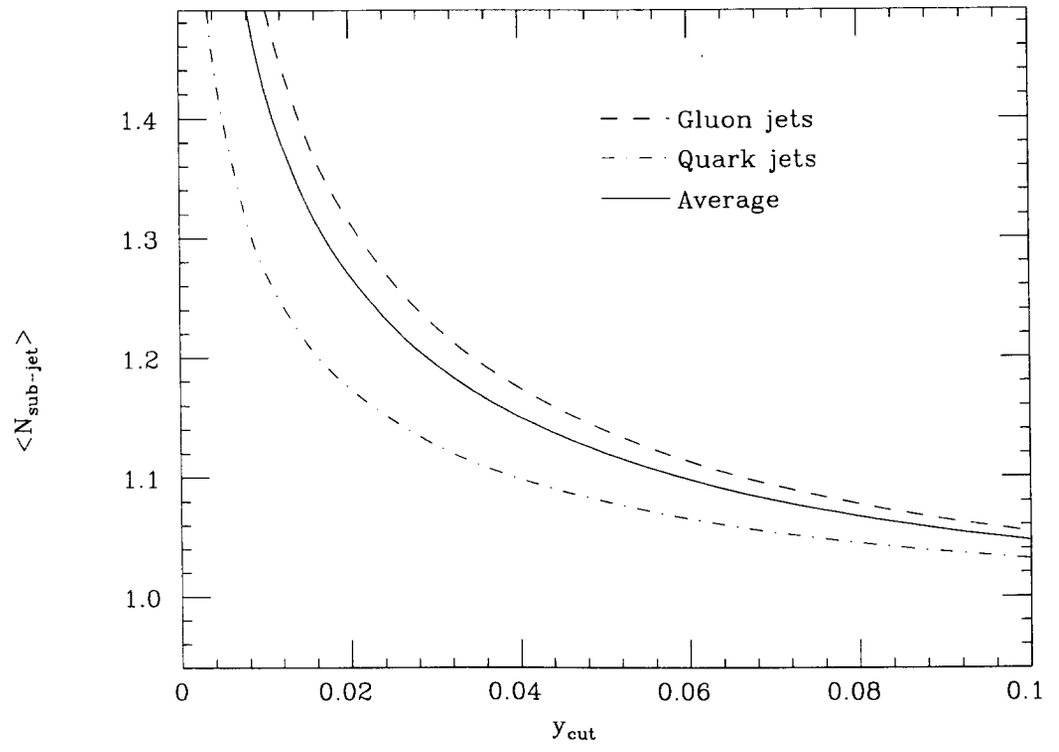

Figure 4a

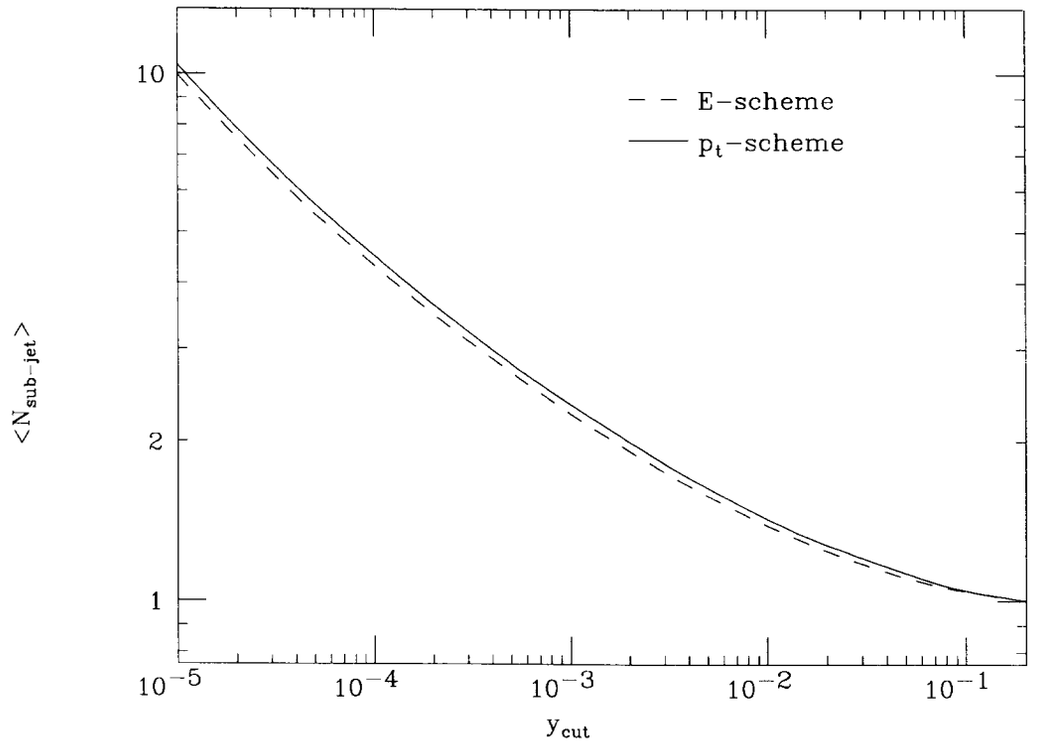

Figure 4b

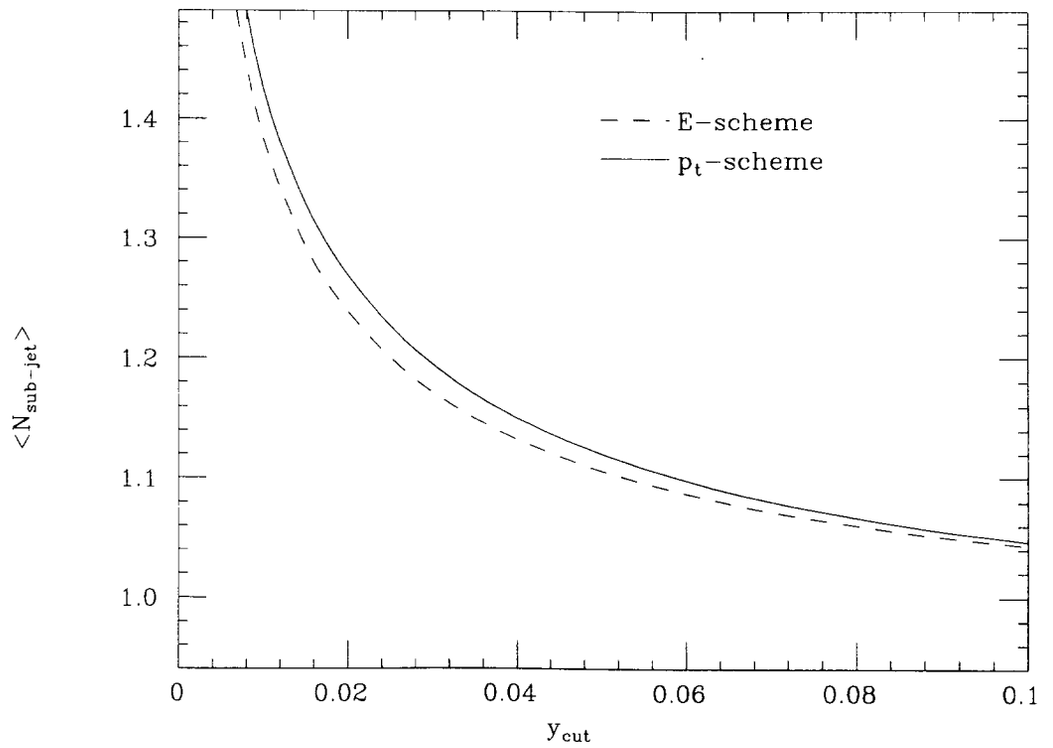

Figure 5

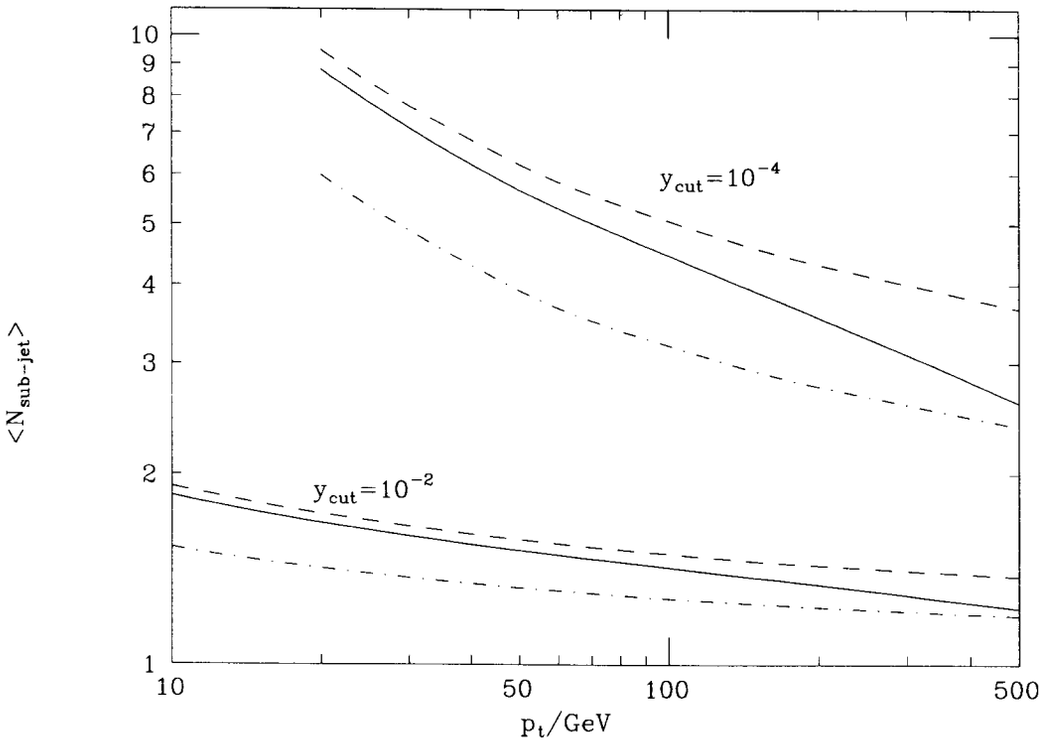

Figure 6

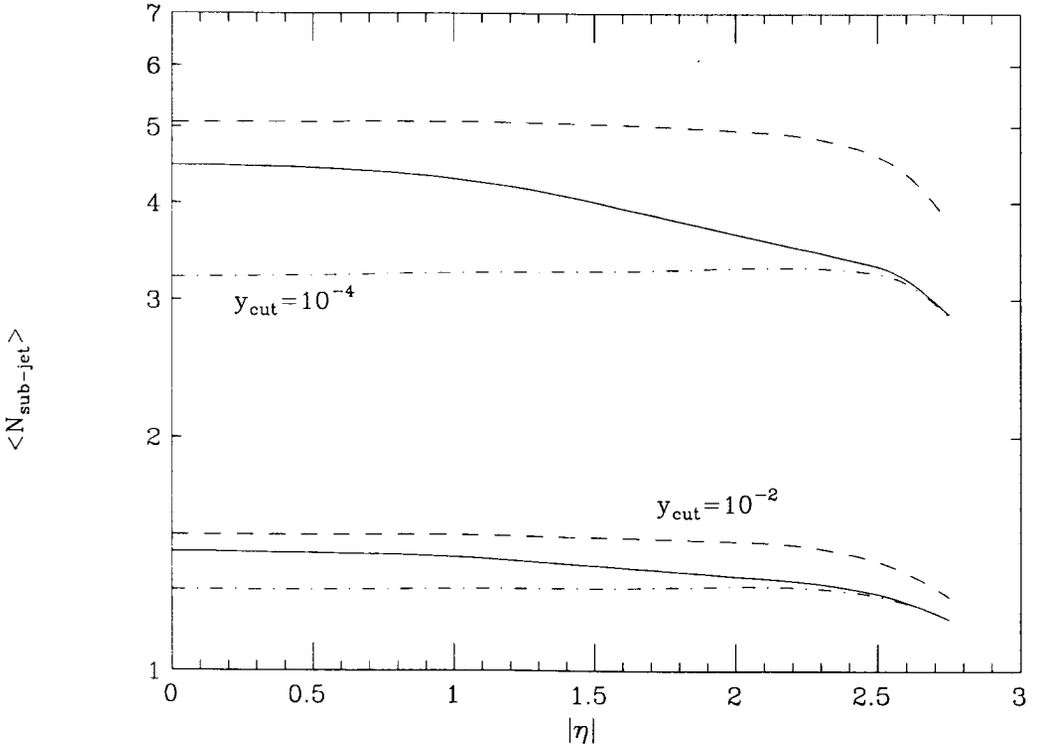

Figure 7

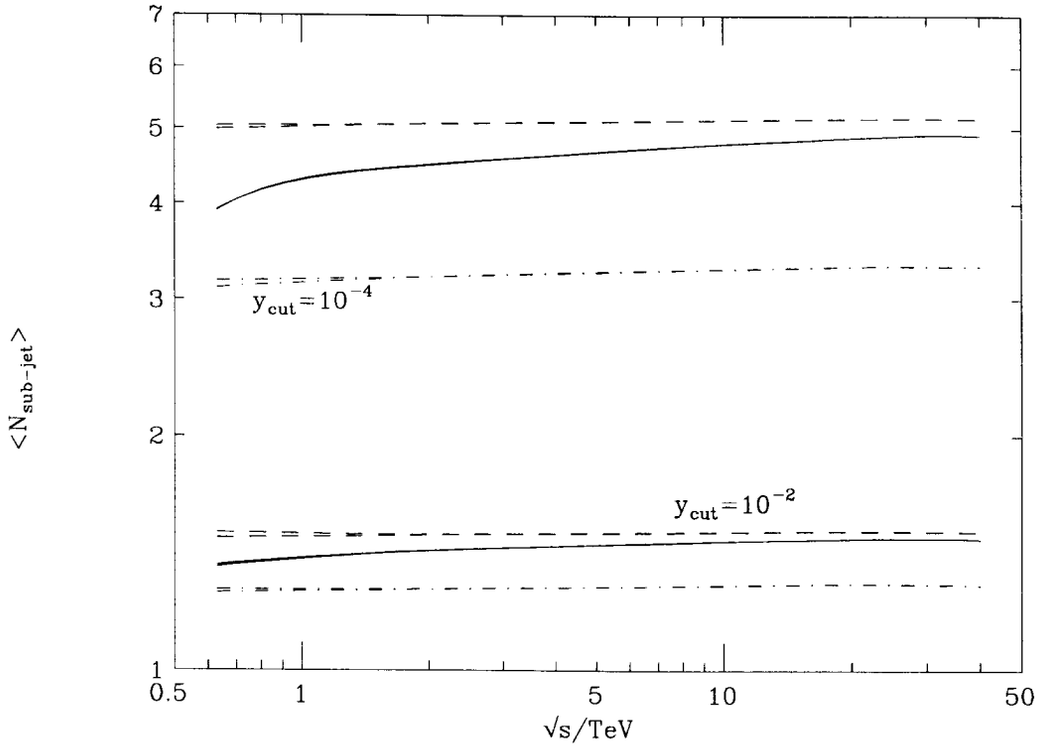

Figure 8